Neurobiology of Disease

Critical Role of Increased PTEN Nuclear Translocation in Excitotoxic and Ischemic Neuronal Injuries

Shu Zhang,[1,2,3] Changiz Taghibiglou,[1] Kimberly Girling,[1] Zhifang Dong,[4] Shinn-Zong Lin,[2] Wei Lee,[2,3] Woei-cherng Shyu,[2,3]* and Yu Tian Wang[1,2,4]*

[1]Brain Research Centre and Department of Medicine, Vancouver Coastal Health Research Institute, University of British Columbia, Vancouver, British Columbia, V6T2B5, Canada, [2]Translational Medicine Research Center and Centers for Neuropsychiatry, China Medical University Hospital, Taichung, 404, Taiwan, [3]Graduate Institute of Immunology, China Medical University, Taichung, 404, Taiwan, and [4]Ministry of Education Key Laboratory of Child Development and Disorders, and Chongqing Key Laboratory of Translational Medical Research in Cognitive Development and Learning and Memory Disorders, Children's Hospital of Chongqing Medical University, Chongqing, China

Stroke is the leading cause of disability in developed countries. However, no treatment is available beyond 3 h post-ictus. Here, we report that nuclear translocation of PTEN (phosphatase and tensin homolog deleted on chromosome TEN) is a delayed step causatively leading to excitotoxic (*in vitro*) and ischemic (*in vivo*) neuronal injuries. We found that excitotoxic stimulation of *N*-methyl-D-aspartate (NMDA) resulted in PTEN nuclear translocation in cultured neurons, a process requiring mono-ubiquitination at the lysine 13 residue (K13), as the translocation was prevented by mutation of K13 or a short interfering peptide (Tat-K13) that flanks the K13 residue. More importantly, using a rat model of focal ischemia, we demonstrated that systemic application of Tat-K13, even 6 h after stroke, not only reduced ischemia-induced PTEN nuclear translocation, but also strongly protected against ischemic brain damage. Our study suggests that inhibition of PTEN nuclear translocation may represent a novel after stroke therapy.

Introduction

Although numerous experimental studies have consistently demonstrated that overactivation of *N*-methyl-D-aspartate (NMDA) receptors (NMDARs) at least partially contributes to excitotoxic/ischemic neuronal damage after stroke (Lucas and Newhouse, 1957; Olney, 1969; Rothman, 1983, 1984; Simon et al., 1984; Lipton and Rosenberg, 1994; Aarts et al., 2002; Arundine and Tymianski, 2004; Lai et al., 2011), the results of clinical trials testing NMDAR antagonists have proven underwhelming (Albers et al., 1995, 1999, 2001; Davis et al., 2000). Although the underlying reasons for this apparent contradiction between basic research results and clinical trials are still unknown, a number of explanations have been postulated, including the short therapeutic time-window of NMDAR antagonists and the significant side effects of these antagonists due to the blockade of the NMDAR's normal functions (Gladstone et al., 2002; Ikonomidou and Turski, 2002; Roesler et al., 2003; Lo, 2008). Therefore, instead of focusing on the receptor, our research instead centers on identifying new molecules and/or pathways downstream of NMDARs specifically involved in mediating excitotoxic/ischemic neuronal death signaling cascades. By focusing our efforts on these targets, we hope to develop new therapeutics possessing a strong post-stroke neuroprotective action, a wider efficacy window, and with greatly reduced side effects.

Phosphatase and tensin homolog deleted on chromosome TEN (PTEN), a dual lipid/protein phosphatase previously identified as an important tumor suppressor (Li et al., 1997; Steck et al., 1997; Maehama and Dixon, 1998; Stambolic et al., 1998), has recently been implicated in contributing to neuronal damage after excitotoxic/ischemic insults (Gary and Mattson, 2002; Ning et al., 2004); however, the underlying mechanisms remain poorly characterized. PTEN′s tumor-suppressive properties are mainly dependent on its lipid phosphatase activity, which antagonizes the cell-survival promoting PI3K/Akt signaling pathway by dephosphorylation of phosphatidylinositol 3,4,5-trisphosphate (PIP_3) (Maehama and Dixon, 1998; Stambolic et al., 1998). As such, a reduction or loss of PTEN′s lipid phosphatase activity has been linked to carcinogenesis in numbers of cancers, including brain, breast, and prostate cancer (Li et al., 1997; Steck et al., 1997; Myers et al., 1998). Interestingly, several recent cancer studies identified two PTEN mutants (K13E and K289E), which retain

Received Dec. 10, 2012; revised March 27, 2013; accepted April 2, 2013.

Author contributions: S.Z., C.T., and Y.T.W. designed research; S.Z., C.T., K.G., Z.D., S.-Z.L., W.L., and W.-C.S. performed research; S.Z., C.T., W.-C.S., and Y.T.W. analyzed data; Y.T.W. wrote the paper.

This work was supported by the Canadian Institutes of Health Research (CIHR), CHDI Foundation, the Taiwan Department of Health Clinical Trial and Research Center of Excellence (DOH102-TD-B-111–004), the National Research Council of Taiwan (NSC100-2632-B-039-001-MY3 and NSC 101-2320-B-039-059-), the National Natural Science Foundation of China 31040085 and 81271221, and Chongqing International Science and Technology Cooperation Foundation cstc201110003. Y.T.W. is a Howard Hughes Medical Institute International Scholar, and Heart and Stroke Foundation of British Columbia and Yukon Chair in Stroke Research. We thank Dr. Alonzo H. Ross (University of Massachusetts Medical School) for PTEN plasmids (GFP-$PTEN_{WT}$, GFP-$PTEN_{K13R}$, NLS-GFP-$PTEN_{WT}$, and NLS-GFP-$PTEN_{C124S}$), Y. P. Auberson (Novartis Pharma AG) for the generous gift from NVP-AAM077, Yuping Li, Dr. Henry Martin, Dr. Lidong Liu, and Dr. Jie Lu for technical support, and Dr. Loren Oschipok and Agnes Kwok for their excellent editorial assistance.

The authors declare no competing financial interests.

*W.-c.S. and Y.T.W. contributed equally to this work.

Correspondence should be addressed to Dr. Yu Tian Wang, Brain Research Centre, 2211 Wesbrook Mall, Vancouver, BC, V6T2B5, Canada. E-mail: ytwang@brain.ubc.ca.

C. Taghibiglou's present address: Department of Pharmacology, University of Saskatchewan, Saskatoon, SK S7N 5E5, Canada.

DOI:10.1523/JNEUROSCI.5661-12.2013

 0270-6474/13/337997-12$15.00/0

normal lipid phosphatase activity but fail to translocate into the nucleus (Georgescu et al., 2000; Walker et al., 2004; Trotman et al., 2007). This reduced nuclear translocation ability impairs PTEN′s tumor suppressing function, leading to reduced apoptotic cell death during tumorigenesis. These findings suggest that nuclear translocation of PTEN may be causally linked to the PTEN′s cell-death promoting activity. Therefore, we hypothesize that increased nuclear PTEN accumulation may occur after excitotoxic/ischemic brain insults, resulting in increased neuronal death, and thereby contributing to excitotoxic/ischemic neuronal damage. Here, we tested this hypothesis using several well characterized *in vitro* and *in vivo* models of excitotoxic/ischemic neuronal injuries.

Materials and Methods

Antibodies and reagents. Mouse anti-PTEN (no. sc-7974) and goat anti-histone deacetylase 1 [(HDAC1) no. sc-6298] were obtained from Santa Cruz Biotechnology. Mouse anti-TATA binding protein [(TBP) no. ab818] and rabbit anti-lamin B1 (no. ab16048) were purchased from Abcam. Mouse anti-Hsp90 (no. 610418) was obtained from BD Transduction Laboratories. Anti-PIP_3 was obtained from Echelon Biosciences. Mouse anti-NeuN (no. MAB377) was purchased from Millipore Corporation. Hoechst 33342 nucleic acid stain, ProLong Gold mounting medium and secondary fluorophore-bound IgGs (Alexa Fluor series) for immunocytochemistry were obtained from Life Technologies. NMDA was purchased from Ascent Scientific. AP5 was purchased from Tocris Bioscience. Complete protease inhibitor cocktail tablets (no. 04693116001) and phosphatase inhibitor cocktail tablets (no. 04906845001) were obtained from Roche Applied Science. Reagents for protein concentration assay (reagent A no. 500-0113, reagent B no. 500-0114) were obtained from Bio-Rad Laboratories. Cell toxicity colorimetric assay kit (LDH assay, no. TOX7) was purchased from Sigma-Aldrich. Nuclear extraction kit was purchased from Panomics (AY2002). Transfection system (calcium phosphate) was purchased from Promega. Tat-fused peptides (Tat-K13, Tat-K13R, and Tat-K289) were custom synthesized by the Peptide Synthesis and Purification Core Facility at University of British Columbia.

Buffers. All buffers were sterilized by autoclaving or vacuum filtration (Corning, polyethersulfone with 0.22 μm pore size). PBS contains 137 mM NaCl, 2.7 mM KCl, 8.1 mM Na_2HPO_4, 1.76 mM KH_2PO_4, pH 7.4. Radio immunoprecipitation assay (RIPA) buffer contains 150 mM NaCl, 0.3% deoxycholic acid sodium, 50 mM Tris, 1 mM EDTA, 1.0% Triton-100, pH 7.4. Four times sample buffer (SB) contains 50% Glycerol, 125 mM Tris-HCl, pH 6.8, 4% SDS, 0.08% bromophenol blue, 5% β-mercaptoethanol. Stripping buffer contains 2% SDS, 62.5 mM Tris-HCl, pH 6.7, 100 mM β-mercaptoethanol. poly-D-Lysine coating solution contains 10 μg/ml poly-D-lysine. HBSS dissection buffer (DB) contains 5.0 g/L glucose, 1.25 g/L sucrose, 0.89 g/L HEPES, pH 7.4, osmolality to 310–320 mOsm, stored at −20°C. Neurobasal plating (NP) media) contains 487.75 ml neurobasal media, 0.5 mM GlutaMAXTM-I supplement, 2% B27 supplement, 25 μm of glutamic acid. Neurobasal feeding (NF) media contains 488.75 ml of neurobasal media, 0.5 mM GlutaMAXTM-I supplement, and 2% B27 supplement.

Plasmids. PTEN plasmids (GFP-$PTEN_{WT}$, GFP-$PTEN_{K13R}$, NLS-GFP-$PTEN_{WT}$, and NLS-GFP-$PTEN_{C124S}$) were kind gifts from Dr. Alonzo H. Ross (University of Massachusetts Medical School). Specifically, the coding sequence of human PTEN was cloned into pcDNA3 plasmid. An enhanced green fluorescent protein (GFP) was inserted into the 5′ end of PTEN to facilitate microscopic visualization. In addition, *N* terminus of GFP-PTEN was fused with a nuclear localization signal (NLS), which can direct the newly synthesized PTEN into the nucleus through the nuclear pore complex. The NLS tag used in the PTEN constructs is SPKKKRKV, which is a strong NLS based on a hexamer protein called SV40 Large T-antigen (Liu et al., 2005). GFP-$PTEN_{K289R}$ plasmid was constructed by site-directed mutagenesis of GFP-$PTEN_{WT}$ using Pfu DNA polymerase. The sequences of all plasmids were confirmed by automated DNA sequencing.

Primary culture of cortical/hippocampal neurons. Pregnant Sprague Dawley rats (E18) were killed by overdosing with 3.5 ml of a 25% urethane solution. Using a dissecting scope, the cortex or hippocampi were isolated and digested with 2–4 ml of prewarmed 0.25% trypsin-EDTA (37°C for 30 min). Then, the dissociated cells were washed with warm DMEM (with 10% FBS) three times, followed by gentle pipetting to ensure a single cell suspension. Next, the cells were resuspended in NP media, counted using a hemocytometer, and plated onto poly-D-lysine-coated culture dishes at a density of 6.0×10^6 per dish (100 mm), 4.0×10^5 per well (12-well plate), or 2.0×10^5 per well (24-well plate). The cells were cultured in a 37°C incubator with 95% O_2 and 5% CO_2. At day 2 *in vitro*, ⅓ NP media was replaced by equal volume of NF media. Media swap was performed every 4 d until cells were used for experiments.

NMDA-induced excitotoxicity. Primary cultures of mature cortical/hippocampal neurons (12–14 DIV) were used in this study. Preliminary tests showed that both cortical and hippocampal neurons reveal very similar results in response to NMDA challenge. Specifically, hippocampal neurons were used in the immunocytochemical experiments, as it is easier to distinguish them from glia cells, whereas cortical neurons were used to provide sufficient material for biochemical experiments. Immediately before NMDA treatment, half of the conditioned medium was taken out and saved for further use. Neurons were stimulated with 25 μm NMDA through bath application, along with other drug/peptide treatments as specified in each individual experiment. After 60 min incubation with NMDA, neurons were washed once with fresh neural basal medium, and then returned to the previously saved conditional medium. Neurons were allowed to recover for different periods of time, ranging from 0 to 24 h until further experiments.

Immunocytochemistry (immunostaining). All imaging experiments were performed double-blind. Neurons cultured on coverslips (in 12-well or 24-well plates) were fixed with 4% paraformaldehyde for 30 min at room temperature, and then incubated with DNA dye Hoechst-33342 (1 μg/ml) for 20 min at room temperature. After three times washing with PBS, the coverslips were mounted onto slides with ProLong Gold mounting medium (Life Technologies). In Figures 1*A* and 2*C*, four visual fields were randomly selected from each coverslip and imaged with a Leica DMIRE2 fluorescence microscope (20× magnification lens, air) and Openlab imaging software (PerkinElmer). The number of apoptotic nuclei and total nuclei were counted, respectively. The condensed or fragmented nuclei were regarded apoptotic, whereas the large and round nuclei were counted as healthy ones. In Figure 1*H*, only neurons with GFP fluorescence (an indicator of successful transfection, 63× magnification lens, oil) were included in neuronal death evaluation. The neuronal death was expressed as a ratio (%) between the number of apoptotic nuclei and that of total nuclei. In Figure 2*A*, the region of the nucleus was defined by overlapping each GFP-PTEN image with its corresponding nucleus DAPI image (63× magnification lens, oil). Nuclear GFP-PTEN and cytoplasmic GFP-PTEN signals were quantified separately by drawing irregular circles around corresponding areas and reading the mean GFP intensities with NIH ImageJ software. The relative nuclear GFP-PTEN level in each neuron was expressed as a ratio between the intensity of nuclear GFP-PTEN and that of cytoplasmic GFP-PTEN from the same cell.

Lactate dehydrogenase assay. Lactate dehydrogenase (LDH) is a cytoplasmic enzyme that can convert nicotinamide adenine dinucleotide (NAD) into NADH (the reduced form). LDH is released from cells into culture medium when the plasma membrane integrity is compromised. Therefore, the amount of released LDH represents the degree of cell death. In this study, the extracellular LDH level was measured using an *in vitro* toxicology assay kit obtained from Sigma-Aldrich (no. TOX-7). The basis of this LDH assay is as follows: (1) LDH reduces NAD into NADH, (2) the resulting NADH is then used in the stoichiometric conversion of a tetrazolium dye, and (3) the resulting colored compound is measured by a spectrophotometric microplate reader at a wavelength of 490 nm. The cell death rate was expressed as a ratio (%) between the absorbance of the treated group and that of the control group.

Nuclei fractionation. Cytoplasm/nuclei fractionation was performed on cultured cortical neurons (6.0×10^6 cells/100 mm dish) or brain tissues by using the Panomics nuclear extraction kit (catalog #AY2002).

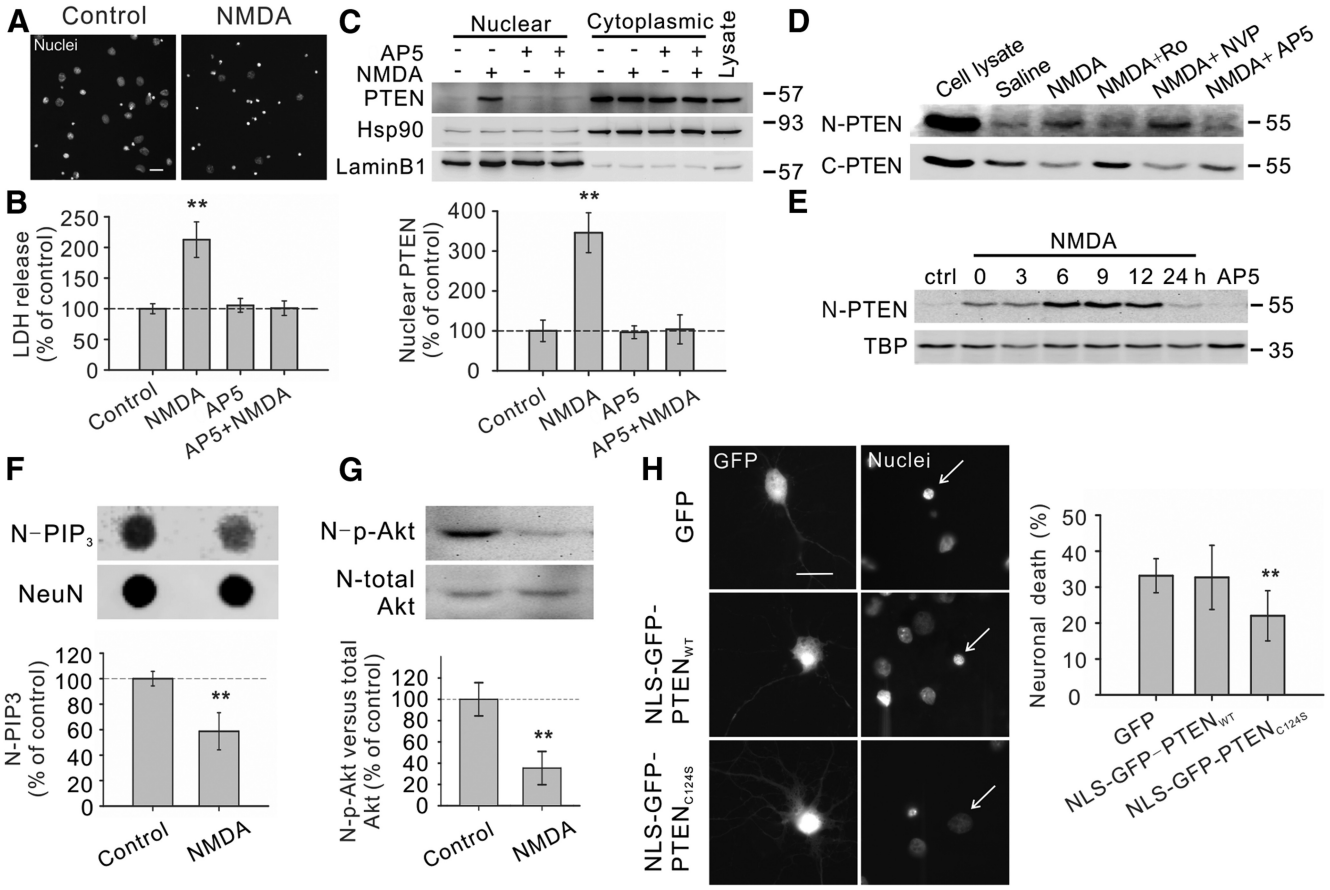

Figure 1. Excitotoxic NMDA stimulation increases PTEN nuclear translocation in cultured neurons. ***A***, ***B***, Bath application of NMDA (25 μm for 1 h, plus 6 h recovery) produced significant neuronal death, as evidenced by the increased numbers of neurons displaying condensed/fragmented nuclei. Scale bar, 20 μm. (Fig. 2*C*, for quantification) and the elevated extracellular levels of LDH (***B***, $n = 7$ culture dishes per group, from 7 independent experiments). The enhanced LDH release could be completely blocked by coapplication of the NMDAR antagonist AP5 (50 μM). ***C***, Western blotting of the cytoplasmic and nuclear fractions showed that NMDA stimulation (25 μm for 1 h, plus 6 h recovery) enhanced PTEN translocation into the nucleus, a process that could be inhibited by AP5 (50 μM). We confirmed the quality of the cytoplasm/nuclei fractionation by sequentially reprobing the blots with cytoplasmic marker Hsp90 and nuclear marker lamin B1. Bar graph at the bottom summarizes data from four independent experiments. ***D***, Western blotting of the nuclear (N-PTEN) and cytoplasmic (C-PTEN) fractions demonstrated that this enhanced PTEN nuclear translocation is primarily mediated by NR2B-containing NMDARs (NR2BRs), as this process could be blocked by NR2B antagonist Ro25-6981 (Ro; 0.5 μM), but not with NR2A-containing NMDAR preferring antagonist NVP-AAM077 (NVP; 0.4 μM). ***E***, Sequential probing of nuclear fractions for PTEN (N-PTEN) and nuclear marker (TBP) showed that the NMDA-induced PTEN nuclear translocation was time-dependent, reaching a peak 6–9 h after stimulation and returning to baseline levels within 24 h; $n = 2$ culture dishes per group, from two independent experiments. It is worth noting that the time course of NMDA-induced PTEN nuclear translocation is slightly different from that induced by ischemia (Fig. 3*A*), probably due to different stimulation intensity. ***F***, Sequential dot blotting of nuclear fractions for PIP_3 (N-PIP_3) and nuclear protein NeuN (NeuN) revealed that the NMDA stimulation (25 μm for 1 h, plus 6 h recovery) caused a marked drop in the nuclear levels of PIP_3, the major physiological substrate of PTEN; $n = 5$ culture dishes per group. ***G***, Sequential blotting of nuclear fractions for phospho-Akt^{Ser473} (N-p-Akt) and total Akt (N-total Akt) revealed that the NMDA treatment (25 μm for 1 h, plus 9 h recovery) caused a dramatic reduction in the nuclear levels of phospho-Akt^{Ser473}; $n = 3$ culture dishes per group. ***H***, Nuclear PTEN activity is critical for NMDA-induced neuronal damage. Images (left) and quantification of neuronal death (right) revealed that NMDA-induced neuronal death, assayed by nuclear condensation at 6 h after NMDA stimulation (25 μm for 1 h), was significantly reduced by overexpression of nucleus-targeted phosphatase-dead PTEN mutant (NLS-GFP-$PTEN_{C124S}$), but not by overexpression of either GFP or nucleus-targeted wild-type PTEN (NLS-GFP-$PTEN_{WT}$); $n = 12$ culture wells in each group, 25 neurons in each culture well were counted, from three independent experiments. Scale bar, 20 μm. Bars represent the group means, and error bars represent SD. *Post hoc* analysis compares treatment groups with control group after significant one-way ANOVA or Kruskal–Wallis on ranks, and significance is defined as $^*p < 0.05$, $^{**}p < 0.01$.

The purity of different cellular fractions was confirmed by probing each fraction for corresponding subcellular marker proteins. As shown in Figure 1*C*, the cytoplasmic marker heat shock protein 90 (Hsp90) primarily localized in the cytoplasmic fraction, whereas the nuclear marker lamin B1 mainly resided in the nuclear fraction, confirming the success of nuclear fractionation.

Western blotting (immunoblotting). Samples consisting of the same amount of total protein (40 μg)were boiled with 4× sample buffer at 95°C for 5 min. The samples were then separated on 10% SDS-PAGE gels and transferred onto polyvinylidene difluoride (PVDF) membranes. To block nonspecific background, the membranes were incubated with 5% fat-free milk for 1 h at room temperature. The target proteins were immunoblotted with primary antibody (overnight at 4°C) and then with corresponding HRP-conjugated secondary antibody (1 h at room temperature). For sequential blotting, the membranes were stripped with stripping buffer, and probed with another antibody. The blots were developed by enhanced chemiluminescence detection system (GE Healthcare), and imaged by Bio-Rad ChemiDoc XRS+ system. The intensities of interested bands (raw data) were quantified using Bio-Rad Quantity One software. If the interested bands were too faint to be viewed, we would adjust the contrast (gamma is never changed) to reveal the bands accordingly. However, such a change in band contrast has no effect on our data quantification as the Quantity One software only analyses the raw data, and not the post-adjusted image. The relative level of target protein is expressed as the percentage between intensity of target protein and that of marker protein on the same blot, such as cytoplasmic marker Hsp90, and nuclear markers including HDAC1, TBP, NeuN, and lamin B1.

Dot blotting. Nuclear extracts were spotted onto nitrocellulose (NC) membranes using Bio-Rad microfiltration apparatus, as instructed by

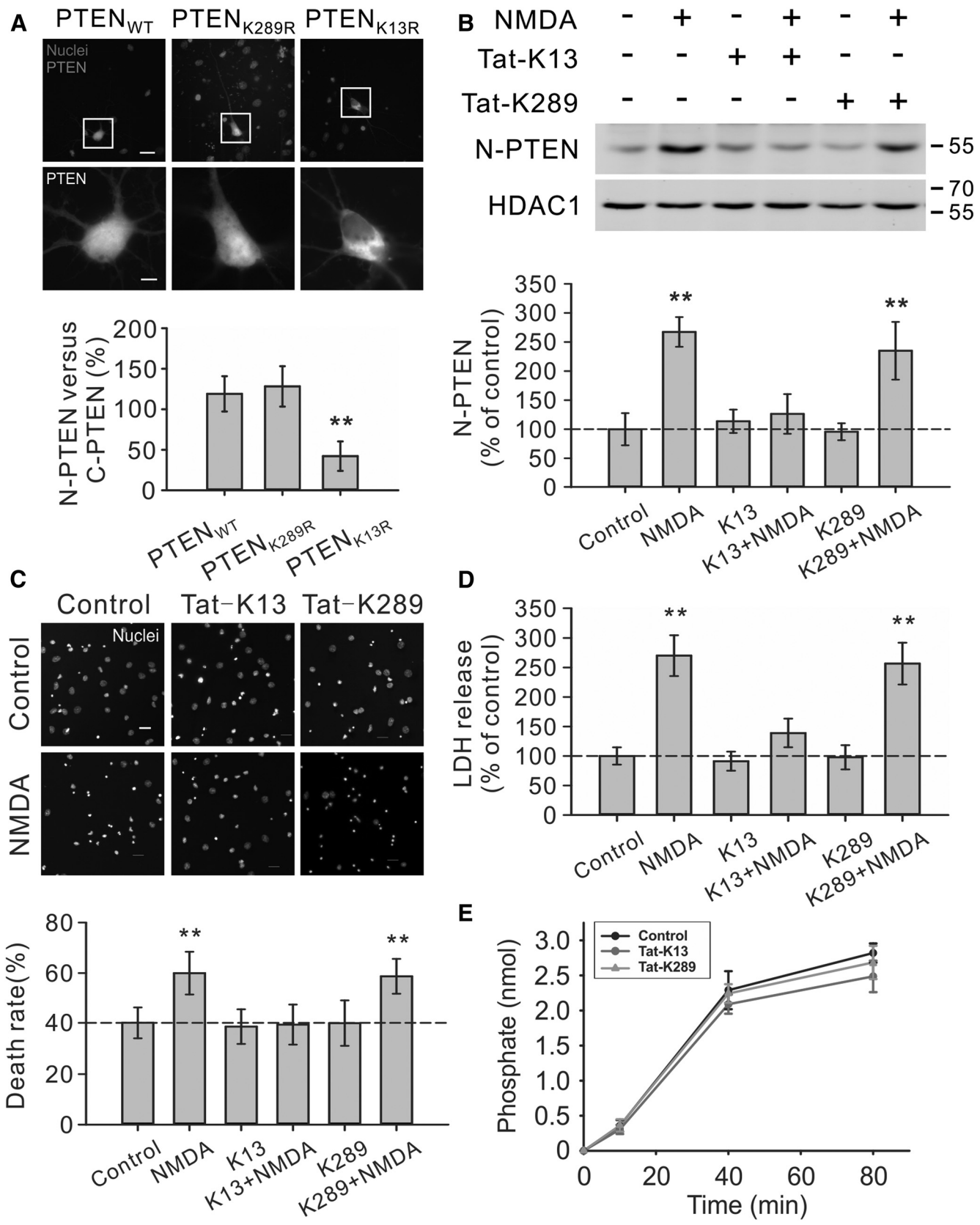

Figure 2. Critical role of PTEN K13 in NMDA-induced PTEN nuclear translocation and neuronal death in cultured neurons. ***A***, K13, but not K289, residue of PTEN is critically important for PTEN nuclear accumulation in neurons. Images (top panels) and nuclear fluorescent intensity qualification (bottom bar graph; $n = 33$ cells per group, from three independent experiments) demonstrated that the GFP signal of GFP-PTEN$_{K13R}$ mutant was predominantly cytoplasmic, being excluded from the nucleus, whereas the GFP signal of either wile type PTEN (GFP-PTEN$_{WT}$) or K289R mutant (GFP-PTEN$_{K289R}$) exhibited a relatively even distribution in both nuclear and cytoplasmic compartments. Scale bar, 20 μm. ***B***, Pretreatment of cultured neurons with interfering peptide Tat-K13 (10 μM), but not Tat-K289 (10 μM), completely blocked the NMDA-stimulated PTEN nuclear translocation as demonstrated by immunoblotting of nuclear fractions ($n = 4$ culture dishes per group, from four independent experiments). Nuclei fractionation was performed at 6 h after NMDA stimulation (25 μm for 1 h). ***C***, ***D***, Tat-K13 prevents NMDA-induced excitotoxicity. (*Figure legend continues.*)

the manufacturer. The NC membranes were blocked with 5% bovine albumin for 60 min at room temperature, washed three times with TBS-T, then probed with an anti-PIP_3 antibody, followed by HRP-labeled secondary antibody. Visualization of the immunoreactive spots was achieved using a chemiluminescent detection system similar to the above Western blotting method, whereas densitometric analysis was performed using NIH ImageJ software. The NC membranes were later stripped and reprobed for nuclear protein NeuN as a loading control.

PTEN phosphatase activity assay. The PTEN phosphatase activity assay was performed in a 96-well flat-bottom clear plate using a commercially available Malachite Green Phosphatase Assay Kit (K-1500, Echelon). The phosphate standards (0 ~ 3 nmol/well), assay controls [buffer control, $PI(3,4,5)P_3$ (PIP_3) only control and PTEN-only control], and PTEN reactions were setup in triplicates. GST-PTEN (100 ng per assay) was added, without or with either peptide Tat-K13 (10 μM) or Tat-K289 (10 μM), to the assay buffer containing substrate PIP_3 (3 nmol per assay) to initiate the reaction. The reaction was allowed to proceed for various periods of 10, 40, or 80 min at 37°C and then terminated with 100 μl of malachite green solution. The green color (free phosphate) was allowed to develop for 20 min at room temperature. The absorbance for the free phosphate was measured at 620 nm in a plate reader. The standard curve was drawn with absorbance (620 nm) on the *y*-axis and phosphate (nmol) on the *x*-axis. A best-fit curve ($Y = A + B \times X + C \times X^2$) was generated by using polynomial second order nonlinear regression analysis. The concentration of free phosphate in each reaction or control was determined by interpolation from the standard curve. The PTEN phosphatase activity was determined by subtracting the background phosphate (average free phosphate value from the "substrate-only" controls) from the phosphate release by PTEN phosphatase action.

Primary culture transfection. Mature hippocampal neurons (10–12 DIV) cultured on coverslips were transfected with target DNA using ProFection Mammalian Transfection System-Calcium Phosphate (Promega, PRE1200). Following transfection, neurons were returned to the incubator for an additional 48 h until further experiments.

Cerebral ischemia. All animals used in the study were housed, cared for, and used experimentally in accordance with the protocols approved by the Ethical Committee for Animal Research at China Medical University Hospital, Taiwan. Adult male Sprague Dawley rats weighting ~200 g were anesthetized, and the middle cerebral artery (MCA) was exposed by making a craniotomy window (2 mm in diameter) 1 mm rostral to the anterior junction of the zygoma and the squamosal bone. The exposed MCA was ligated with a square knot using a 10-0 nylon suture. Next, the bilateral common carotid arteries (CCAs) were clamped with nontraumatic arterial clips. Successful surgery was confirmed by a marked drop in regional cerebral blood flow, monitored by a laser Doppler flowmeter (PF-5010, Periflux system; Perimed AB). Moreover, the core body temperature was monitored with a thermometer probe (Hewlett-Packard Model 21090A probe), and maintained at 37.0 ± 0.5°C with a heating pad. Both blood pressure and blood gas levels were also monitored during the experiment. After 90 min ischemia, the suture and clips were removed to allow instant reperfusion. Experimental rats were subdivided into several groups to receive different treatments of interfering peptides (Tat-K13, Tat-K13R, or Tat-K289 at a dosage of 10 mg/kg) or saline via femoral vein injection. The first bolus of Tat-K13 was administered at either 2 or 6 h after stroke onset, whereas Tat-K13R, Tat-K289, and saline were given at 2 h after stroke onset. To achieve the optimal outcome, another two doses of peptides were administered on the second and third days, respectively. Rats were then allowed to recover for different periods of time until additional experiments.

Magnetic resonance image. The rats were anesthetized and the body temperature was kept at 37.0 ± 0.5°C with a heating pad during imaging process. The T2-weighted spin-echo imaging sequence (T2WI) was performed by the 3.0 T General Electric imaging system (R4, GE) with the following parameters: repetition time, 4000 ms; echo time, 105 ms; 6–8 contiguous coronal slices with each 2 mm thick. At this stage of stroke development (7 d post-ischemia), brain infarct manifests as high signal (bright white) on the magnetic resonance image (MRI) images. The noninfarct areas were drawn manually from slice to slice and the volumes were measured with Voxtool analysis software (General Electric). The infarct size was quantified by subtracting the noninfarct volume of the ischemic hemisphere from the total volume of the contralateral hemisphere.

[^{18}F]fluoro-2-deoxyglucose positron emission tomography examination. ^{18}F was produced by the ^{18}O(p, n)^{18}F nuclear reaction in a cyclotron, and ^{18}F-FDG ([^{18}F]fluoro-2-deoxyglucose) was synthesized with an automated ^{18}F-FDG synthesis system (Nihon Kokan) at China Medical University and Hospital, Taiwan. The positron emission tomography (PET) scanning was performed by a high-resolution small-animal PET scanner (microPET, Rodent R4, Concorde Microsystems) with the system parameters described previously (Carmichael et al., 2004). At day 7 post-stroke surgery, rats were anesthetized and fixed in a customized stereotactic head holder in the microPET scanner. The rats were then given a bolus intravenous injection of ^{18}F-FDG (200–250 μCi/rat) dissolved in 0.5 ml of saline. Immediately following the ^{18}F-FDG administration, rats were subjected to PET scanning for 60 min using a 3-D acquisition protocol (Shyu et al., 2008). Data collected were analyzed by Interactive Data Language (IDL) ver. 5.5 (Research Systems) and ASIPro ver. 3.2 (Concorde Microsystems). Last, the deficit of brain glucose metabolic activity was expressed using the following formula: [1-ipsilateral hemisphere signal/contralateral hemisphere signal] × 100%.

Neurological behavioral tests. Three typical sensorimotor deficit assessments were designed to evaluate the functional recovery of neural circuits damaged by ischemic insult. They are the biased body swing test, locomotor activity test, and grip strength test. Biased body swing test is a measurement of body asymmetric motor behavior. It was performed by elevating the rat by its tail and counting the frequency of its swing behavior. Previous studies revealed that ischemic rats exhibit a significantly biased swing activity with the direction contralateral to the ischemic side, whereas the native rats have no preference for either side. Therefore, the frequency of the biased swing activity may represent the degree of neurological deficits caused by ischemic stroke. The detailed experimental design is as follows. The rat was lifted to ~1 inch above the floor by its tail. One swing behavior was counted when the rat moved its head >10° from the vertical axis to either the contralateral side or ipsilateral side of ischemia. Twenty continuous swings were counted in total, and the percentage of recovery was normalized using the following formula: percentage recovery = [1 − (No. of contralateral swings − 10)/10] × 100%. Locomotor activity of the ischemic rats was monitored using the VersaMax Animal Activity Monitor obtained from Accuscan Instruments. The monitor has 16 horizontal *x-y* and eight vertical *z* infrared sensors spaced 2.5 cm apart. The vertical sensors were situated 10 cm from the floor of the chamber. The ischemic rat was placed in the recording chamber at night, and its vertical movement time (seconds) was automatically recorded by computer when the infrared beams were broken by its movement over a 2 h period. The length of its vertical movement represents the recovery of locomotor circuits injured by ischemic stroke. Grip strength is another index for testing motor functions. It was recorded by a grip strength meter manufactured by TSE Systems. Briefly, the rat was mounted onto the grip sensor and pulled backwards gently by its tail with a continuous movement. Naturally, the rat clung to the grip sensor firmly to resist the pull until it could no longer hold on and let it go. The maximum force at which the animal released the grip was recorded by the grip strength meter. Twenty pulls were performed for both left forelimb and right

←

(*Figure legend continued.*) Tat-K13 (10 μM), but not the control peptide Tat-K289 (10 μM), decreased the number of neurons displaying nuclei condensation/fragmentation (***C***, $n = 8$ culture wells per group, from three independent experiments, four visual fields were randomly selected from each culture well and averaged; scale bar, 20 μm) and reduced LDH release (***D***, $n = 27$ culture wells per group, from three independent experiments). Both assays were performed at 6 h after NMDA stimulation (25 μm for 1 h). ***E***, *In vitro* PTEN lipid phosphatase activity assays revealed that within the concentration tested (10 μM), neither the interfering peptide Tat-K13 nor the control peptide Tat-K289 had significant effects on the production of free phosphates from the lipid substrate PIP_3 by recombinant PTEN ($n = 3$). Bars represent the group means, and error bars represent SD. *Post hoc* analysis compares treatment groups with control group after significant one-way ANOVA or Kruskal–Wallis on ranks, and significance is defined as $^*p < 0.05$, $^{**}p < 0.01$.

forelimb, respectively, and the readings were averaged to get the mean grip strength for each forelimb. The strength of the impaired forelimb (contralateral to stroke side) was calculated as the percentage of the intact forelimb's performance (ipsilateral to stroke side). Then, the improvement of motor function was expressed as the ratio between the grip strength measured at 28 d (post-test) and that measured at 1 d (pre-test) following middle cerebral artery ligation surgery.

Statistical analysis. All data were tested for normality distribution fitting by the Shapiro–Wilk test and for equal variance by Levene median test. When values were normally distributed and groups had identical variance, we used a one-way ANOVA, followed by Tukey's HSD *post hoc* test when appropriate. When data did not meet the above ANOVA assumptions, we used nonparametric ANOVA (Kruskal–Wallis one-way ANOVA on ranks) for multiple-group comparisons and Mann–Whitney rank sum test for two-sample comparison. Data were expressed as mean ±SD. Statistical significance was defined as $^{*}P < 0.05$, $^{**}P < 0.01$.

Results

Excitotoxic NMDA stimulation increases PTEN nuclear translocation in cultured neurons

To determine whether excitotoxic stimulation increases nuclear translocation of PTEN, we used a NMDA-induced excitotoxicity protocol in cultured cortical neurons *in vitro* using two independent neuronal death assays, nuclear staining and LDH release (Fig. 1*A*,*B*). Nuclear staining of neurons can reveal nuclei condensation/fragmentation, which is one of the most commonly used indicators for cell apoptosis (Hardingham et al., 2002; Wang et al., 2004), whereas the LDH assay can allow for the nonbiased quantitative identification of both apoptotic and necrotic neuronal damage (Koh and Choi, 1987; Liu et al., 2007). As previously reported (Liu et al., 2007; Taghibiglou et al., 2009), NMDA (25 μM; 1 h) resulted in significant neuronal damage as evidenced by the increased numbers of neurons with condensed/fragmented nuclei (Figs. 1*A*, 2*C* for quantification) and the elevated extracellular levels of LDH, 6 h after stimulation (Kruskal–Wallis one-way analysis on ranks, $H_3 = 15.217$, $p = 0.002$) (Fig. 1*B*). The NMDA-induced neuronal damage is mediated through NMDARs, as the increased LDH release was blocked by coapplication of the NMDAR antagonist AP5 (50 μM) (NMDA, 212.6 ± 29.0% of control, $n = 7$ culture dishes per group, from seven independent experiments, Dunn's Method, versus control, $p < 0.01$; AP5 + NMDA, 100.9 ± 11.9%, $n = 7$, versus control, $p > 0.05$) (Fig. 1*B*).

Next, we investigated whether this NMDA challenge results in an increase in PTEN nuclear translocation using cytoplasm/nuclei fractionation techniques and Western blotting. To confirm the successful separation of the respective cytoplasmic and nuclear fractions, blots were reprobed with corresponding cytoplasmic and nuclear protein markers, heat shock protein 90 (Hsp90) and lamin B1, respectively (Fig. 1*C*). The results revealed that stimulation of cultured neurons with NMDA produced a marked increase in nuclear PTEN levels, a process which could be prevented by coapplication of the NMDAR antagonist AP5 (50 μM) (one-way ANOVA, $F_{(3,12)} = 50.318$, $P < 0.001$; NMDA, 345.9 ± 50.0% of control, $n = 4$ culture dishes per group, from four independent experiments, Tukey's HSD test, versus control, $p < 0.001$; AP5 + NMDA, 103.7 ± 36.3%, $n = 4$, versus control, $p = 0.999$) (Fig. 1*C*). This enhanced PTEN nuclear translocation is primarily mediated by neuronal death-associated NR2B-containing NMDA receptors (NR2BRs), as PTEN nuclear translocation was blocked by pretreatment with the NR2BR antagonist Ro25–6981 (0.5 μM), but not affected by inhibition of the survival-promoting NR2A-containing NMDA receptors (NR2ARs) with the NR2AR antagonist NVP-AAM077 (0.4 μM) (Fig. 1*D*) (Liu et al., 2007; Okamoto et al., 2009; Tu et al., 2010; Lai et al., 2011). This is consistent with a potential role for NMDAR-induced PTEN nuclear translocation in mediating excitotoxic neuronal injuries. Moreover, a detailed time course study revealed that the NMDA-induced PTEN nuclear translocation was time-dependent, reaching a peak 6–9 h after treatment, and returning to control levels within 24 h ($n = 2$ culture dishes per group, from two independent experiments) (Fig. 1*E*). Thus, PTEN nuclear translocation appears to be a delayed signaling cascade downstream of activation of NR2B-containing NMDARs.

PTEN nuclear translocation is an essential step leading to NMDAR-mediated neuronal death

As a lipid phosphatase, a major function of PTEN is to convert $PI(3,4,5)P_3$ into $PI(4,5)P_2$, hence antagonizing the PI3 kinase/Akt cell survival signaling pathways (Maehama and Dixon, 1998; Lee et al., 1999). Consequently, one can expect that NMDA-induced PTEN nuclear translocation may result in an alteration in the nuclear levels of PIP_3 and Akt activity (that could be gauged by the levels of phosphorylated Akt). Consistent with this conjecture, we observed a marked drop in nuclear PIP_3 levels 6 h after NMDA treatment (NMDA, 58.7 ± 14.6% of control, $n = 5$ culture dishes, Mann–Whitney Rank Sum, $U = 0.000$, $T = 40.000$, $p = 0.008$) (Fig. 1*F*), and a dramatic reduction in nuclear levels of phospho-Akt^{Ser473} versus total Akt at 9 h post-NMDA stimulation (NMDA, 33.2 ± 12.4% of control, $n = 3$ culture dishes, *t* test, $t = 6.579$ with 4 degrees of freedom, $p = 0.003$) (Fig. 1*G*). The results not only provide further evidence for NMDA-induced PTEN nuclear translocation, but also suggest that nuclear PTEN, like its cytoplasmic counterpart, may function as a lipid phosphatase of PIP_3 in the nucleus and hence negatively regulate the nuclear pool of PI3K-Akt cell survival promoting signaling pathways. To further address whether the phosphatase activity of nuclear PTEN causatively contributes to NMDA-induced excitotoxic neuronal damage, we next examined NMDA excitotoxicity in cultured neurons transfected with either wild-type GFP-$PTEN_{WT}$ or a phosphatase-dead mutant GFP-$PTEN_{C124S}$ (Maehama and Dixon, 1998). For these constructs to be preferentially expressed in the nucleus, both constructs were fused to a well characterized classic NLS (Liu et al., 2005). NLS can direct its fusion protein into the nucleus to achieve nuclear enrichment. As shown in Figure 1*H*, nuclear overexpression of the phosphatase-dead PTEN (NLS-GFP-$PTEN_{C124S}$) functioned as a dominant negative inhibitor, reducing NMDA-induced excitotoxicity as demonstrated by the significant decrease in the nuclear condensation/fragmentation of these transfected neurons in comparison with those transfected with either wild-type PTEN or control plasmid GFP (one-way ANOVA, $F_{(2,33)} = 9.483$, $P < 0.001$; GFP, 33.2 ± 4.7% neuronal death, $n = 12$ culture wells per group, 25 neurons in each culture well were counted, from three independent experiments; NLS-GFP-$PTEN_{WT}$, 32.7 ± 8.9%, $n = 12$; NLS-GFP-$PTEN_{C124S}$, 22.0 ± 7.0%, $n = 12$; Tukey's HSD test, GFP versus NLS-GFP-$PTEN_{C124S}$, $p = 0.002$; NLS-GFP-$PTEN_{WT}$ versus NLS-GFP-$PTEN_{C124S}$, $p = 0.002$) (Fig. 1*H*). Thus, the increased PTEN nuclear translocation following NMDA stimulation appears an essential step leading to NMDA-induced excitotoxic neuronal damage.

Recent studies using a number of cancer cell lines provide strong evidence supporting a critical role of mono-ubiquitination of lysine residues K13 and K289 in mediating PTEN nuclear accumulation (Trotman et al., 2007; Wang et al., 2007). To investigate whether these two lysine residues are also

essential for neuronal PTEN nuclear translocation, neurons were transfected with PTEN mutants containing a lysine-to-arginine mutation at either lysine residue (K13R and K289R). As shown in Figure 2*A*, in neurons transfected with either the wild-type PTEN ($GFP\text{-}PTEN_{WT}$) or K289R mutant ($GFP\text{-}PTEN_{K289R}$), the GFP signal exhibited a relatively even distribution in both nuclear and cytoplasmic compartments ($GFP\text{-}PTEN_{WT}$, the ratio between nuclear and cytoplasmic PTEN signal being 119.0 ± 21.8%, n = 33 neurons per group, from three independent experiments; $GFP\text{-}PTEN_{K289R}$, 128.2 ± 24.9%, n = 33) (Fig. 2*A*). In contrast, in neurons transfected with the K13R mutation ($GFP\text{-}PTEN_{K13R}$), the GFP signal was predominantly cytoplasmic, being excluded from the nucleus ($GFP\text{-}PTEN_{K13R}$, 42.1 ± 18.2%, n = 33; Kruskal–Wallis one-way analysis on ranks, $H_2 = 64.507$, $P = < 0.001$; *post hoc* Tukey's HSD test, $GFP\text{-}PTEN_{WT}$ versus $GFP\text{-}PTEN_{K289R}$, $p > 0.05$; $GFP\text{-}PTEN_{WT}$ versus $GFP\text{-}PTEN_{K13R}$, $p < 0.01$) (Fig. 2*A*). These results strongly suggest that unlike previous observations in cancer cell lines (Trotman et al., 2007; Wang et al., 2007), only the K13 residue (but not the K289 residue) appears critically important for PTEN nuclear accumulation in neurons.

To further confirm the essential role of K13 residue in NMDA-induced PTEN nuclear localization, we next designed two interfering peptides that flank the K13 residue ($KEIVSRNK_{13}RRYQED$) and K289 residue ($GPEETSEK_{289}VENGS$) of PTEN, respectively. We hypothesize that the K13 peptide may competitively inhibit PTEN mono-ubiquitination at the K13 residue, and hence block PTEN nuclear translocation in neurons. In contrast, as the K289 residue is not required for PTEN nuclear translocation in neurons (Fig. 2*A*), the K289 peptide may not affect PTEN nuclear translocation. Both peptides were rendered membrane permeable by fusion of them with the cell-membrane transduction domain of the human immunodeficiency virus-type 1 (HIV-1) Tat protein (GRKKRRQRRR) (Schwarze et al., 1999; Aarts et al., 2002; Borsello et al., 2003; Taghibiglou et al., 2009). Consistent with our predictions, the results of nuclei/cytoplasm fractionation on primary neuronal cultures demonstrated that the NMDA-triggered PTEN nuclear accumulation could be abolished by Tat-K13 coapplication (10 μM), but not by Tat-K289 (10 μM) (one-way ANOVA, $F_{(5,18)} = 23.809$, $p < 0.001$; NMDA, 267.3 ± 25.5% of control, n = 4 culture dishes per group, from four independent experiments, Tukey's HSD test, versus control, $p < 0.001$; K13+NMDA, 126.2 ± 34.1%, n = 4, versus control, $p = 0.828$; K289 + NMDA, 234.0 ± 49.6%, n = 4, versus control, $p < 0.001$) (Fig. 2*B*). These results further confirm that the K13 residue (but not the K289 residue) is critically important for NMDA-induced PTEN nuclear translocation in neurons, and indicate that the Tat-K13 peptide is an effective inhibitor for blocking PTEN nuclear translocation.

The ability of Tat-K13 to efficiently prevent NMDA-induced PTEN nuclear translocation suggests that it may be an effective neuroprotectant for excitotoxic neuronal injuries. We first tested this in neuronal cultures undergoing NMDA-induced excitotoxic neuronal damage using both nuclear condensation (Fig. 2*C*) and LDH release (Fig. 2*D*) assays. Our results revealed that pretreatment of the cultured neurons with Tat-K13 (10 μM), but not Tat-K289 (10 μM), prevented the NMDAR-mediated neuronal damage. As shown in Figure 2*C*, NMDA treatment triggered a significant increase in the percentage of neurons displaying condensed/fragmented nuclei (one-way ANOVA, $F_{(5,42)} = 14.254$, $p < 0.001$; control, 40.3 ± 6.1% neuronal death, n = 8 culture wells per group, from three independent experiments; NMDA, 60.0 ± 8.4%, n = 8; Tukey's HSD test, $p < 0.001$) (Fig. 2*C*). This enhanced apoptosis was blocked by pretreatment of neurons with Tat-K13, but not with Tat-K289 (K13+NMDA, 39.6 ± 7.9%, n = 8, versus control, $p = 1.000$; K289+NMDA, 58.7 ± 6.9%, n = 8, versus control, $p < 0.001$) (Fig. 2*C*). Moreover, evidence from the LDH assay also confirmed that Tat-K13 possessed a strong neuroprotective effect against NMDA insult (Kruskal–Wallis one-way analysis on ranks, $H_5 = 128.957$, $P = < 0.001$) (Fig. 2*D*). The NMDA-triggered LDH release was prevented by coapplication of Tat-K13, but not Tat-K289 (NMDA, 270.0 ± 34.6% of control, n = 27 culture wells per group, from 3 independent experiments, Tukey's HSD test, versus control, $p < 0.01$; K13+NMDA, 139.0 ± 24.2%, n = 27, versus control, $p > 0.05$; K289+NMDA, 256.5 ± 35.4%, n = 27, versus control, $p < 0.01$) (Fig. 2*D*). To further confirm that the neuroprotective effect of Tat-K13 is primarily mediated by inhibiting the PTEN nuclear translocation rather than affecting PTEN′s lipid phosphatase activity in the cytoplasm, we conducted an *in vitro* PTEN lipid phosphatase activity assay using the malachite green method. The results showed that within the concentration tested (10 μM), neither the interfering peptide Tat-K13 nor the control peptide Tat-K289 had any notable effect on the lipid phosphatase activity of PTEN toward PIP_3, suggesting that the newly developed Tat-K13 interfering peptide likely represents a novel therapeutic neuroprotectant which may avoid potential side effects due to altering enzymatic functions of PTEN (Fig. 2*E*).

Enhanced PTEN nuclear translocation contributes to ischemic neuronal injuries following a focal ischemic brain insult *in vivo*

As excessive activation of NMDARs is regarded as one of the major causes for neuronal injuries during ischemic stroke (Lucas and Newhouse, 1957; Olney, 1969; Rothman, 1983, 1984; Simon et al., 1984; Lipton and Rosenberg, 1994; Aarts et al., 2002; Arundine and Tymianski, 2004; Lai et al., 2011), we next tested whether PTEN nuclear translocation occurs following ischemic brain insults, and if so, whether Tat-K13 can prevent the ischemia-induced PTEN nuclear translocation, thereby reducing ischemia-induced neuronal injury. Here, we used a well characterized *in vivo* rat stroke model, which involves transient occlusion of the distal MCA (Chen et al., 1986; Shyu et al., 2008).

To test whether an ischemic insult can trigger PTEN nuclear translocation *in vivo*, rats were challenged with a 90 min transient ischemic event, then allowed to recover for various periods of time ranging from 2 to 24 h post-ictus. Nuclear fractionation assays revealed a time-dependent increase in PTEN nuclear accumulation in the brain tissues of the ischemic area containing both the core and penumbra regions, when compared with the corresponding area from the contralateral brain region (Fig. 3*A*). The levels of nuclear PTEN in the ischemic brain area gradually increased following ischemic challenge, reaching a peak at 12 h and returning to baseline levels within 24 h after stroke onset (Fig. 3*A*, right).

To determine whether the Tat-K13 following systemic application can prevent the ischemic nuclear PTEN translocation and hence reduce the ischemic neuronal injuries, we first tested whether Tat-K13, following systemic application, could enter neurons in the ischemic penumbra using a fluorophore-tagged peptide Tat-K13-carboryfluorescein. As shown in Figure 3*B*, this fluorescent Tat-K13 (10 mg/kg, i.v.) administered 6 h after stroke onset not only effectively entered the brain, but was enriched in neurons in the infarct area within 1 h following application (Fig. 3*B*). This apparent enrichment in the infarct brain area is likely due to a transient increase in blood–brain-Barrier leakage following ischemic insults (Belayev et al., 1996; Fernandez-Lopez et al., 2012) These results indicate that post-stroke systemic admin-

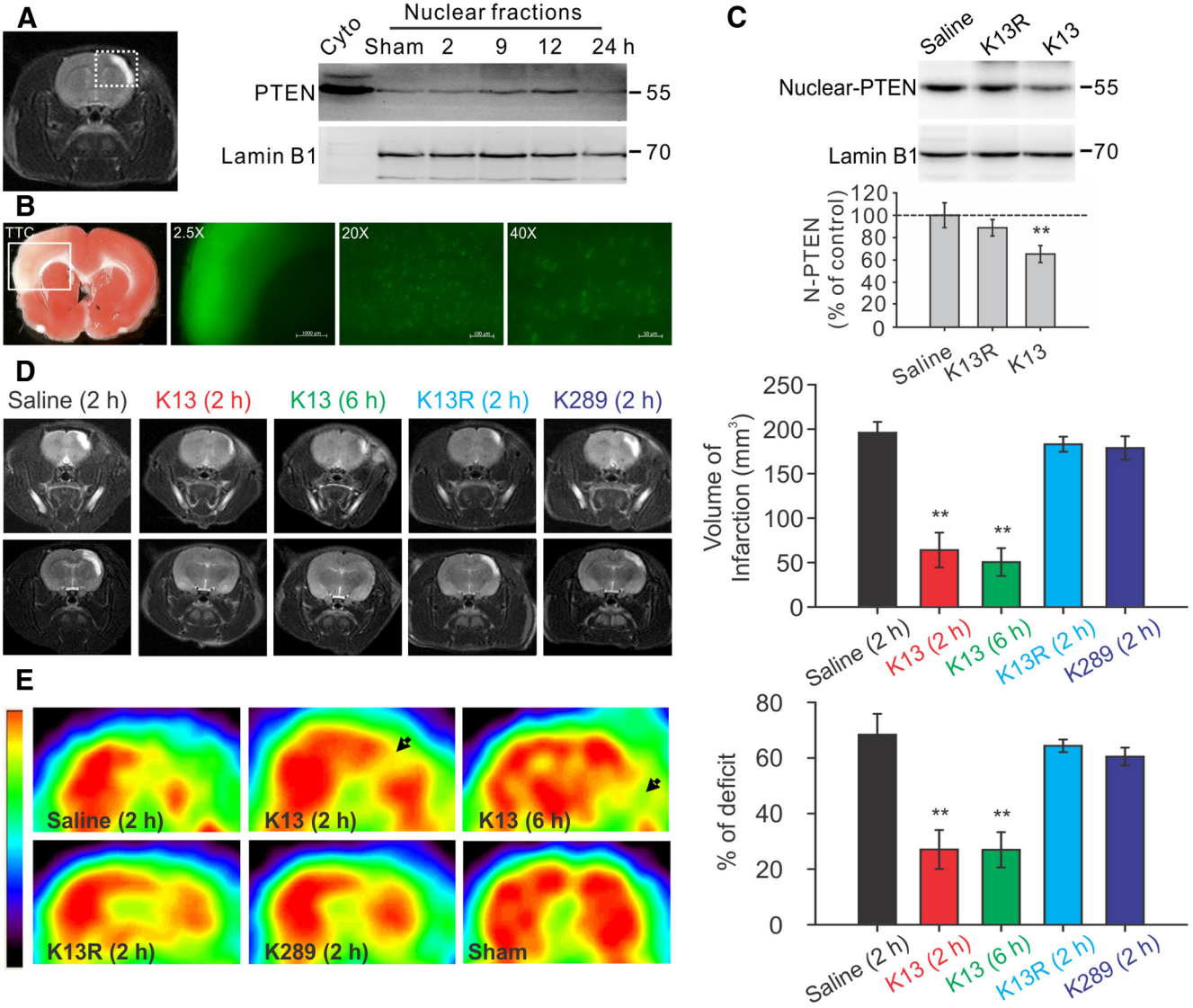

Figure 3. Enhanced PTEN nuclear translocation contributes to ischemic neuronal injuries following a focal ischemic brain insult *in vivo*. Mature Sprague Dawley rats were challenged with a 90 min focal ischemic event by a transient ligation of the right MCA and bilateral CCAs, and then allowed to recover for various periods of time as indicated. ***A***, Ischemic insult triggered a time-dependent PTEN nuclear translocation in the infarct cortical area. Left, Representative coronal scanning image of MRI taken at day 7 from a saline-treated control stroke rat showed a well defined infarct (white) area. Right, Sequential probing of nuclei fractions for PTEN and nuclear protein lamin B1 from the infarct areas (the white square area indicated on the left) taken at various time points following stroke, showed a time-dependent increase in PTEN nuclear translocation, which reached a peak 12 h after stroke and returned to baseline levels within 24 h ($n = 2$ rats per group). ***B***, Systemic application of Tat-K13 effectively entered neurons in the brain, including neurons in the ischemic penumbra region. Fluorescent peptide Tat-K13-Carboryfluorescein (10 mg/kg, i.v.) was applied 6 h after stroke insult, and brain sections were processed 1 h after the peptide administration. Left, The image of triphenyltetrazolium chloride (TTC) staining (1-mm-thick coronal brain section) revealed an observable infarct area in the sensorimotor cortex in the insult side of the brain. Right, Fluorescent microscopic images were taken from sections immediately adjacent to the TTC stained section on the left. The image (taken at 2.5× magnification) of the infarct area in a 1-mm-thick brain section corresponds to the area indicated by the white box in the TTC section on the Left, and showed that the peptide not only entered the brain, but also appeared to be particularly enriched in the infarct region. Images of a 20-μm-thick brain section of the infarct region taken at high magnifications (20× or 40×) further confirmed the successful transduction of the peptide into individual cells in the ischemic area. ***C***, Application of Tat-K13 peptide at 6 h after ictus reduced the stroke-triggered PTEN nuclear translocation. Sequential probing of nuclei fractions for PTEN (N-PTEN) and nuclear protein lamin B1 from the infarct regions showed that Tat-K13 (K13; 10 mg/kg, i.v.), but not its control Tat-K13R (K13R; 10 mg/kg, i.v.), significantly decreased the ischemia-induced PTEN nuclear translocation when assayed at 12 h after stroke ($n = 6$ rats per group). ***D***, Representative MRI scanning images from rostral (top) to caudal (bottom) levels were taken at day 7 from rats subjected to a 90 min transient focal ischemic insults and received various treatments as indicated. Bar graph on the right summarizes results from 10 rats in each group. Tat-K13 (K13; 10 mg/kg, i.v.) given at either 2 or 6 h after stroke-onset significantly reduced infarct areas in comparison with the control peptide Tat-K13R (K13R; 10 mg/kg, i.v.) or Tat-K289 (K289; 10 mg/kg, i.v.), or saline administered at 2 h after stroke onset. ***E***, FDG-PET scanning taken at day 7 from the same groups of animals in ***D*** revealed a striking recovery in brain glucose metabolic activities in the infarct areas of animals receiving Tat-K13 in comparison with that in animals receiving the control peptide Tat-K13R or Tat-K289, or saline. The color scale (left) represents relative levels of glucose metabolism, from high (red) to low (blue). Bars represent the group means, and error bars represent SD. *Post hoc* analysis compares treatment groups with control (saline) group after significant one-way ANOVA or Kruskal–Wallis on ranks, and significance is defined as $*p < 0.05$, $**p < 0.01$.

istration could effectively deliver this peptide into neurons in the ischemic/infarct regions of the brain.

Having proved the effective delivery of the peptide into ischemic regions, we next tested whether the Tat-K13 peptide could inhibit the ischemia-induced PTEN nuclear translocation *in vivo*. As most stroke patients arrive at hospital several hours after stroke onset, any clinically relevant treatment should have therapeutic efficacy even when given several hours after stroke onset. Given that PTEN nuclear accumulation peaks ~12 h post-ictus (Fig. 3*A*) and Tat-peptide administered through intravenous in-

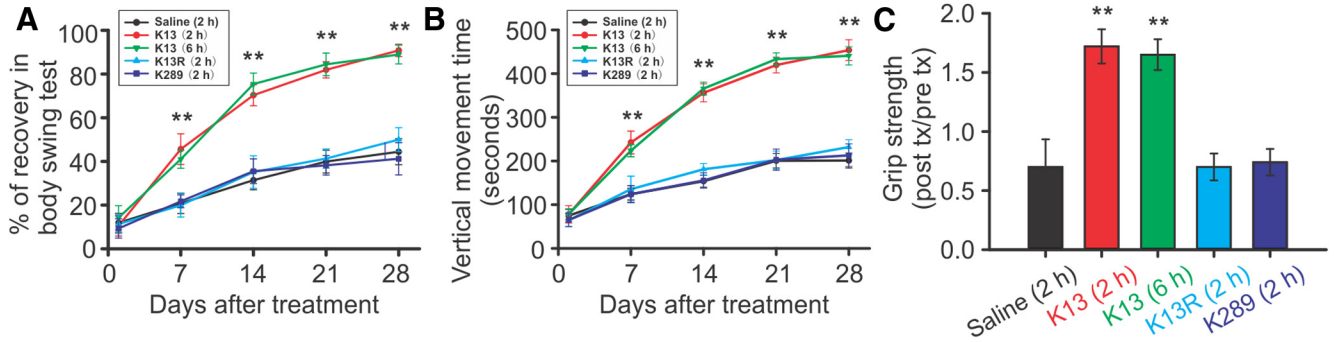

Figure 4. Post-stroke treatment with Tat-K13 peptide improves motor behavioral performances after a focal ischemic brain insult *in vivo*. Focal ischemia and peptide applications were as described in Figure 3 ($n = 10$ in each group). ***A***, Biased body swing tests revealed that animals receiving post-stroke treatment of Tat-K13 (both 2 and 6 h groups) exhibited a much faster recovery than those treated with saline or control peptides over the 4 week recovery period following stroke. ***B***, Tat-K13 peptide, but not its control peptides, dramatically promoted the locomotor activity recovery of the stroke rats in comparison with saline treatment. The locomotor activity (vertical movement time) was automatically measured using a computerized locomotor box within a 2 h observation period over the 4 week recovery period following stroke. ***C***, The grip strength test showed that animals receiving Tat-K13 treatments (both 2 and 6 h groups) had a much better grip strength performance than those receiving control peptides or saline at 28 d after stroke. Together, these behavioral tests suggest a long-lasting therapeutic effect of Tat-K13 peptide on improving the motor functions. Bars represent the group means, and error bars represent SD. *Post hoc* analysis compares treatment groups with control (saline) group after significant one-way ANOVA or Kruskal–Wallis on ranks, and significance is defined as $*p < 0.05$, $**p < 0.01$.

jection can quickly reach therapeutic concentrations in the brain within 1 h (Fig. 3*B*) (Aarts et al., 2002; Taghibiglou et al., 2009; Cook et al., 2012), systemic application of Tat-K13 at 6 h post-ictus should allow a sufficient time to inhibit the major portion of the ischemia-induced PTEN nuclear translocation. To further confirm the specificity of Tat-K13 peptide, we also developed another control peptide Tat-K13R in which the lysine 13 residue (K13) was replaced with an arginine (R13). The conversation of K13 into R13 should render Tat-K13R incapable of competing with endogenous PTEN mono-ubiquitination on the K13 site, and hence function as an inactive control for Tat-K13. As predicted, intravenous application of Tat-K13, but not Tat-K13R (10 mg/kg, i.v.) at 6 h after stroke onset significantly suppressed the ischemia-induced PTEN nuclear translocation when assayed 12 h after stroke onset (one-way ANOVA, $F_{(2,15)} = 24.033$, $P < 0.001$) (Fig. 3*C*). Nuclear PTEN levels in the Tat-K13-treated rats was reduced to 65.3 ± 7.6% of the saline-treated group, whereas nuclear PTEN levels in the Tat-K13R-treated rats were statistically similar to saline controls (saline, $n = 6$ rats per group; K13, $n = 6$; Tukey's HSD test, $p < 0.001$; K13R, 88.8 ± 7.3% of saline control, $n = 6$, versus control, $p = 0.106$) (Fig. 3*C*). These results confirmed that PTEN nuclear translocation is a relatively delayed cellular process following stroke onset, one that can be inhibited by a post-stroke treatment with Tat-K13.

To examine the causative link between ischemia-induced PTEN nuclear translocation and ischemic neuronal death, we inhibited PTEN nuclear translocation with systemic intravenous administration of Tat-K13, or with Tat-K13R or Tat-K289 serving as controls. We administered the first dose of Tat-K13 (10 mg/kg, i.v.) to treatment groups at either 2 or 6 h post-ictus, and gave Tat-K13R or Tat-K289 (10 mg/kg, i.v.) to control groups at 2 h post-ictus. To increase the efficacy of the peptide, we also gave two additional doses of each peptide at days 2 and 3 following stroke. The long-lasting morphological neuroprotective effects of the peptides were then assessed using MRI 7 d after stroke onset. As shown in Figure 3*D*, MRI scanning revealed that rats treated with Tat-K13, regardless of whether it was given at 2 or 6 h post-ictus, had dramatically reduced brain infarct volumes compared with saline-treated rats (Kruskal–Wallis one-way analysis on ranks, $H_4 = 38.639$, $P = < 0.001$; saline control, 170.9 ± 18.7 mm^3, $n = 10$ rats per group; K13 (2 h), 67.7 ± 17.5 mm^3, $n = 10$, Tukey's HSD test, versus saline, $p < 0.01$; K13 (6 h), 67.4 ± 15.9 mm^3, $n = 10$, versus saline, $p < 0.01$) (Fig. 3*D*). In contrast, post-ictus treatment of control peptides (Tat-K13R and Tat-K289), displayed little protective effects against ischemia-induced brain infarction [K13R (2 h), 160.9 ± 5.7 mm^3, $n = 10$, versus saline, $p > 0.05$; K289 (2 h), 151.2 ± 8.0 mm^3, $n = 10$, versus saline, $p > 0.05$] (Fig. 3*D*).

We then examined whether Tat-K13 also provides a corresponding functional protection of neurons from the ischemic insults by measuring the recovery of neuronal glucose uptake with FDG-PET 7 d after stroke onset. Consistent with the MRI results, FDG-PET scanning also revealed a significant recovery in FDG uptake deficits in the ischemic hemisphere in the two groups of rats treated with Tat-K13 in comparison with rats treated with saline [one-way ANOVA, $F_{(4,45)} = 246.269$, $p < 0.001$; saline control, 78.4 ± 4.8% deficit, $n = 10$ rats per group; K13 (2 h), 25.6 ± 7.8% deficit, $n = 10$, Tukey's HSD test, versus saline, $p < 0.001$; K13 (6 h), 20.2 ± 6.3% deficit, $n = 10$, versus saline, $p < 0.001$] (Fig. 3*E*). In contrast, no obvious recovery was observed in rats treated with either control peptide [K13R (2 h), 73.2 ± 3.4% of deficit, $n = 10$, versus saline, $p = 0.267$; K289 (2 h), 71.5 ± 5.3% of deficit, $n = 10$, versus saline, $p = 0.07$] (Fig. 3*E*). Together, MRI and PET acquisitions suggest that Tat-K13, by blocking PTEN nuclear accumulation, strongly protects neurons against ischemic injuries.

It is clinically important to know whether a neuroprotectant, in addition to providing neuronal protection, will have a long-lasting behavioral benefit in stroke patients. We therefore also examined whether the post-stroke Tat-K13 treatments provide neurobehavioral benefits using three typical sensorimotor assessments, the biased body swing, locomotor activity, and grip strength measurements, which are often used to evaluate the functional recovery of cortical neural circuits damaged by focal ischemic insult (Dunnett et al., 1998; Chang et al., 2003; Shyu et al., 2008). Over the 4 week recovery period following stroke challenge, the body swing test revealed that rats treated with Tat-K13 (both 2 and 6 h groups) exhibited a much faster recovery in the body asymmetric motor behavior than those treated with saline or either of the control peptides (Fig. 4*A*). By day 28, rats treated with Tat-K13 had largely recovered from the body asymmetry deficit [Kruskal–Wallis one-way analysis on ranks, $H_4 = 38.017$, $P = < 0.001$; saline control, 44.4 ± 6.0% recovery, $n = 10$ rats per group; K13 (2 h), 90.8 ± 2.8% recovery, $n = 10$, Tukey's HSD

test, versus saline, $p < 0.01$; K13 (6 h), 88.9 ± 4.3% recovery, $n = 10$, versus saline, $p < 0.01$] (Fig. 4*A*). In contrast, those treated with either control peptide (Tat-K13R or Tat-K289) had similar performance as the saline controls [K13R (2 h), 50.0 ± 5.4% recovery, $n = 10$, versus saline, $p > 0.05$; K289 (2 h), 41.2 ± 7.4% recovery, $n = 10$, versus saline, $p > 0.05$] (Fig. 4*A*). Similarly, the vertical movement time as monitored in a computerized locomotor chamber showed that Tat-K13-treated rats (both 2 and 6 h groups) displayed a much faster and more dramatic improvement in locomotor activity over the 4 week recovery period in comparison with the saline-treated or control peptide-treated rats (Fig. 4*B*). On day 28, a one-way ANOVA analysis indicated a significant difference among the groups (one-way ANOVA, $F_{(4,45)} = 361.269$, $p < 0.001$). *Post hoc* comparisons (Tukey's HSD test) revealed that the vertical movement time of Tat-K13-treated rats was significantly longer than that of saline-treated rats [saline control, 200.9 ± 17.2 s, $n = 10$ rats per group; K13 (2 h), 453.6 ± 23.7 s, $n = 10$, versus saline, $p < 0.001$; K13 (6 h), 440.6 ± 20.7 s, $n = 10$, versus saline, $p < 0.001$] (Fig. 4*B*). On the other hand, the locomotor activity was unaffected by control peptide treatments [K13R (2 h), 231.8 ± 16.8 s, $n = 10$, versus saline, $p = 0.018$; K289 (2 h), 213.0 ± 26.1 s, $n = 10$, versus saline, $p = 0.708$] (Fig. 4*B*). Furthermore, results of the grip strength test also revealed a more dramatic recovery in rats treated with Tat-K13 at 28 d after stroke (Kruskal–Wallis one-way analysis on ranks, $H_4 = 35.840$, $P = < 0.001$) (Fig. 4*C*). Tat-K13 treatment, regardless at 2 or 6 h post-ictus, dramatically enhanced the grip strength recovery compared with saline treatment, whereas control peptides exhibited no protective effect [saline control, 0.70 ± 0.23 post/pre grip strength, $n = 10$ rats per group; K13 (2 h), 1.72 ± 0.14, $n = 10$, Tukey's HSD test, versus saline, $p < 0.01$; K13 (6 h), 1.65 ± 0.13, $n = 10$, versus saline, $p < 0.01$; K13R (2 h), 0.70 ± 0.11, $n = 10$, versus saline, $p > 0.05$; K289 (2 h), 0.74 ± 0.11, $n = 10$, versus saline, $p > 0.05$] (Fig. 4*C*). Together, our results in the rat model of stroke strongly indicate that Tat-K13 not only reduces brain infarct size, but also improves the functional neurological circuits damaged by ischemic insults.

Discussion

Our present study identifies increased PTEN nuclear translocation as an essential step in signaling cascades leading to NMDAR/ischemia-mediated neuronal injuries. We provide several pieces of evidence supporting a causative role of PTEN nuclear translocation in mediating neuronal injuries: (1) PTEN nuclear translocation is downstream of a NR2B-containing NMDAR mediated cell death signaling pathway (Fig. 1*D*) (Lai et al., 2011); (2) nuclear overexpression of dominant negative mutant PTEN reduces NMDAR-mediated excitotoxicity (Fig. 1*H*); and (3) most importantly, specific blockade of PTEN nuclear translocation with the Tat-K13 peptide prevents NMDAR-mediated excitotoxicity in cultured neurons (Fig. 2) and protects against ischemic brain damage *in vivo* (Figs. 3, Fig. 4). Thus, increased PTEN nuclear translocation appears an essential step leading to excitotoxic/ischemic neuronal death. Our study is in agreement with a recent report that reduction in nuclear PTEN import promotes nuclear TDP-43-mediated neuronal survival (Zheng et al., 2012). Moreover, our study is also consistent with two recent reports on axonal regenerative and neuroprotective effects of PTEN ablation (Domanskyi et al., 2011; Sun et al., 2011). The advantage of the neuroprotection induced by Tat-K13 peptide over PTEN ablation methods is that Tat-K13 does not interfere with the cytoplasmic functions of PTEN, whereas deletion of PTEN abrogates all of its functions. It is interesting to note that a recent study using Nedd4 family-interacting protein 1 (Ndfip1) conditional knock-out animals also reported a parallel reduction in PTEN nuclear translocation and an increase in neuronal vulnerability following ischemic insults (Howitt et al., 2012). However, as an E3 ligase adaptor protein, knock-out of Ndfip1 would not only affect PTEN, but numerous substrates of the E3-ligase Nedd4. Thus, it is most likely that the increased neuronal vulnerability observed in Ndfip1$^{-/-}$ is due to its impact on one or more cell survival signaling pathways, rather than decreasing PTEN nuclear translocation.

It is also significant to note that several recent studies also reported an essential role of PTEN nuclear translocation in PTEN′s tumor suppressing function. Using several cancer cell lines and human cancer specimens, these studies demonstrated that impaired PTEN nuclear translocation causally contributes to tumorigenesis of various types of cancers (Georgescu et al., 2000; Gimm et al., 2000; Whiteman et al., 2002; Walker et al., 2004; Trotman et al., 2007). Recent studies on human glioblastoma and Cowden's disease identified two PTEN mutants (K13E and K289E) which retain normal lipid phosphatase activity but fail to translocate into the nucleus, leading to impaired PTEN tumor suppressing ability during tumorigenesis (Georgescu et al., 2000; Walker et al., 2004; Trotman et al., 2007). Even more strikingly, in the thyroid, normal follicular cells are characterized by stronger PTEN staining in the nucleus than in the cytoplasm, whereas the nuclear staining intensity of PTEN progressively diminishes during progression from normal to follicular adenoma to carcinoma (Gimm et al., 2000). A similar trend has also been observed in melanoma progression (Whiteman et al., 2002). These results, along with that presented in this work, clearly establish that normal function of PTEN nuclear translocation is a critical mechanism in regulating cell survival and death, one that is shared between tumorigenesis and neurodegeneration. Impaired PTEN nuclear translocation may lead to the failure in suppression of cell growth, contributing to the pathogenesis of various cancers. On the other hand, overexaggerated PTEN nuclear translocation can enhance cell death, leading to neurodegeneration. Thus, further characterization of how PTEN nuclear translocation regulates cell survival and death may lead to a better understanding of the mechanisms underlying the pathogenesis of both tumorigenesis and neurodegeneration.

Our current study revealed an essential role of PTEN nuclear translocation in mediating excitotoxic and ischemic neuronal death. However, the detailed mechanisms by which nuclear PTEN increases the vulnerability of neurons to excitotoxicity and ischemia remain unclear. Evidence from previous cancer studies suggests that nuclear PTEN may function as a nuclear PIP_3 phosphatase and consequently antagonize nuclear PI3K/Akt prosurvival signaling pathways (Gimm et al., 2000; Deleris et al., 2003; Ahn et al., 2004, 2005; Vasko et al., 2004). In pheochromocytoma cells (PC12), nuclei extracts pretreated with purified PTEN showed increased DNA fragmentation in response to apoptotic stimulation, which could be rescued by an oversupply of PIP_3 (Ahn et al., 2004, 2005). Moreover, during thyroid tumorigenesis, the level of nuclear PTEN was found to be inversely correlated to that of activated nuclear Akt during the progression from the normal thyroid follicular cells to adenoma to carcinoma (Gimm et al., 2000; Vasko et al., 2004). These results are in harmony with our observation that NMDA stimulation resulted in a sharp drop in nuclear levels of PIP_3 and phospho-Akt, and this NMDA-induced neurotoxicity was inhibited by nuclear overexpression of dominant negative mutant $PTEN_{C124S}$. Therefore, it is very plausible to speculate that nuclear PTEN may mediate excitotoxic

neuronal death through antagonizing nuclear PIP_3/Akt survival signaling pathways. In addition, nuclear PTEN may exert its neurotoxic actions via a PIP_3-independent mechanism. Recent studies found that PTEN can form a physical complex with p53 in the nucleus, thereby protecting p53 from ubiquitination-mediated degradation and facilitating p53-dependent apoptosis (Freeman et al., 2003; Tang and Eng, 2006). Further examination of the detailed mechanisms by which PTEN nuclear translocation increases neuronal vulnerability may lead to the identification of novel targets for developing therapeutic neuroprotectants.

The mechanisms mediating excitotoxic/ischemic neuronal death are complicated processes, and multifactors and steps have been suggested (Lipton, 1999; Lai et al., 2011). The rather striking neuroprotective effectiveness of PTEN nuclear translocation inhibition raises an interesting question as how to relate PTEN nuclear translocation to these molecules and steps previously implicated in excitotoxic/ischemic signaling pathways. Because PTEN nuclear translocation is a relatively delayed step causing ischemic neuronal damage (reaching a peak at 12 h post-ictus), PTEN might be a later common step where several NMDAR down-stream signaling cascades, including early cytosolic signaling molecules such as NR2B-PSD95 (Jurado et al., 2010) and later nuclear factors, such as TPD-43 (Zheng et al., 2012), converge to induce neuronal damage. This could partially explain why the Tat-K13 peptide has an effective post-stroke therapeutic window of >6 h. Furthermore, it is significant to point out that in addition to NMDAR-mediated excitotoxicity, PTEN nuclear translocation is also a critical step in non-NMDAR-mediated cell death mechanisms (Freeman et al., 2003; Chung and Eng, 2005; Tang and Eng, 2006; Shen et al., 2007). Increasing evidence supports the idea that some non-NMDAR-mediated mechanisms, such as free radical generation and p53 overactivation (whether secondary to or independent of NMDAR activation), may contribute significantly to brain damage, particularly following severe stroke insults (Lipton, 1999; Aarts et al., 2002; Leker et al., 2004). Thus, by blocking these non-NMDAR-dependent cell death mechanisms, inhibition of PTEN nuclear translocation may not only have a wider therapeutic window, but may also be more effective than some of the previously reported NMDAR-based post-stroke neuroprotective manipulations (Lai et al., 2011).

Through characterization of the mechanisms underlying NMDAR-mediated PTEN nuclear translocation, we developed a peptide (Tat-K13) as a specific PTEN nuclear translocation inhibitor and demonstrated that it may represent a novel effective stroke treatment. As observed using both MRI and PET imaging, it provides long-lasting morphological and functional protection of neurons against ischemic insults. Moreover, behavioral analysis further proves its ability to promote behavioral recovery. Unlike most NMDAR antagonism-based neuroprotectants previously tested in stroke clinical trials (Albers et al., 1995, 1999, 2001; Davis et al., 2000), Tat-K13 does not affect NMDARs, but targets PTEN nuclear translocation, a delayed step in the NMDAR-mediated cell death signaling cascade. Therefore, Tat-K13 likely has a much wider post-stroke therapeutic window, with reduced side effects. Finally, as NMDAR-mediated excitotoxicity is thought to contribute to the pathogenesis of a large number of chronic neurodegenerative disorders (such as Alzheimer's and Huntington's diseases to mental illnesses) in addition to acute brain insults, such as stroke and brain trauma (Lipton and Rosenberg, 1994), this study may have broad implications beyond stroke.

References

Aarts M, Liu Y, Liu L, Besshoh S, Arundine M, Gurd JW, Wang YT, Salter MW, Tymianski M (2002) Treatment of ischemic brain damage by perturbing NMDA receptor-PSD-95 protein interactions. Science 298: 846–850. CrossRef Medline

Ahn JY, Rong R, Liu X, Ye K (2004) PIKE/nuclear PI 3-kinase signaling mediates the antiapoptotic actions of NGF in the nucleus. EMBO J 23: 3995–4006. CrossRef Medline

Ahn JY, Liu X, Cheng D, Peng J, Chan PK, Wade PA, Ye K (2005) Nucleophosmin/B23, a nuclear PI(3,4,5)P(3) receptor, mediates the antiapoptotic actions of NGF by inhibiting CAD. Mol Cell 18:435–445. CrossRef Medline

Albers GW, Atkinson RP, Kelley RE, Rosenbaum DM (1995) Safety, tolerability, and pharmacokinetics of the *N*-methyl-D-aspartate antagonist dextrorphan in patients with acute stroke: dextrorphan study group. Stroke 26:254–258. CrossRef Medline

Albers GW, Clark WM, Atkinson RP, Madden K, Data JL, Whitehouse MJ (1999) Dose escalation study of the NMDA glycine-site antagonist licostinel in acute ischemic stroke. Stroke 30:508–513. CrossRef Medline

Albers GW, Goldstein LB, Hall D, Lesko LM (2001) Aptiganel hydrochloride in acute ischemic stroke: a randomized controlled trial. JAMA 286: 2673–2682. CrossRef Medline

Arundine M, Tymianski M (2004) Molecular mechanisms of glutamate-dependent neurodegeneration in ischemia and traumatic brain injury. Cell Mol Life Sci 61:657–668. CrossRef Medline

Belayev L, Busto R, Zhao W, Ginsberg MD (1996) Quantitative evaluation of blood-brain barrier permeability following middle cerebral artery occlusion in rats. Brain Res 739:88–96. CrossRef Medline

Borsello T, Clarke PG, Hirt L, Vercelli A, Repici M, Schorderet DF, Bogousslavsky J, Bonny C (2003) A peptide inhibitor of c-Jun *N*-terminal kinase protects against excitotoxicity and cerebral ischemia. Nat Med 9:1180–1186. CrossRef Medline

Carmichael ST, Tatsukawa K, Katsman D, Tsuyuguchi N, Kornblum HI (2004) Evolution of diaschisis in a focal stroke model. Stroke 35:758–763. CrossRef Medline

Chang CF, Lin SZ, Chiang YH, Morales M, Chou J, Lein P, Chen HL, Hoffer BJ, Wang Y (2003) Intravenous administration of bone morphogenetic protein-7 after ischemia improves motor function in stroke rats. Stroke 34:558–564. CrossRef Medline

Chen ST, Hsu CY, Hogan EL, Maricq H, Balentine JD (1986) A model of focal ischemic stroke in the rat: reproducible extensive cortical infarction. Stroke 17:738–743. CrossRef Medline

Chung JH, Eng C (2005) Nuclear-cytoplasmic partitioning of phosphatase and tensin homologue deleted on chromosome 10 (PTEN) differentially regulates the cell cycle and apoptosis. Cancer Res 65:8096–8100. CrossRef Medline

Cook DJ, Teves L, Tymianski M (2012) Treatment of stroke with a PSD-95 inhibitor in the gyrencephalic primate brain. Nature 483:213–217. CrossRef Medline

Davis SM, Lees KR, Albers GW, Diener HC, Markabi S, Karlsson G, Norris J (2000) Selfotel in acute ischemic stroke: possible neurotoxic effects of an NMDA antagonist. Stroke 31:347–354. CrossRef Medline

Déléris P, Bacqueville D, Gayral S, Carrez L, Salles JP, Perret B, Breton-Douillon M (2003) SHIP-2 and PTEN are expressed and active in vascular smooth muscle cell nuclei, but only SHIP-2 is associated with nuclear speckles. J Biol Chem 278:38884–38891. CrossRef Medline

Domanskyi A, Geissler C, Vinnikov IA, Alter H, Schober A, Vogt MA, Gass P, Parlato R, Schutz G (2011) Pten ablation in adult dopaminergic neurons is neuroprotective in Parkinson's disease models. FASEB J 25:2898–2910. CrossRef Medline

Dunnett SB, Torres EM, Annett LE (1998) A lateralised grip strength test to evaluate unilateral nigrostriatal lesions in rats. Neurosci Lett 246:1–4. CrossRef Medline

Fernández-López D, Faustino J, Daneman R, Zhou L, Lee SY, Derugin N, Wendland MF, Vexler ZS (2012) Blood-brain barrier permeability is increased after acute adult stroke but not neonatal stroke in the rat. J Neurosci 32:9588–9600. CrossRef Medline

Freeman DJ, Li AG, Wei G, Li HH, Kertesz N, Lesche R, Whale AD, Martinez-Diaz H, Rozengurt N, Cardiff RD, Liu X, Wu H (2003) PTEN tumor suppressor regulates p53 protein levels and activity through phosphatase-dependent and-independent mechanisms. Cancer Cell 3:117–130. CrossRef Medline

Gary DS, Mattson MP (2002) PTEN regulates Akt kinase activity in hippocampal neurons and increases their sensitivity to glutamate and apoptosis. Neuromolecular Med 2:261–269. CrossRef Medline

Georgescu MM, Kirsch KH, Kaloudis P, Yang H, Pavletich NP, Hanafusa H (2000) Stabilization and productive positioning roles of the C2 domain of PTEN tumor suppressor. Cancer Res 60:7033–7038. Medline

Gimm O, Perren A, Weng LP, Marsh DJ, Yeh JJ, Ziebold U, Gil E, Hinze R, Delbridge L, Lees JA, Mutter GL, Robinson BG, Komminoth P, Dralle H, Eng C (2000) Differential nuclear and cytoplasmic expression of PTEN in normal thyroid tissue, and benign and malignant epithelial thyroid tumors. Am J Pathol 156:1693–1700. CrossRef Medline

Gladstone DJ, Black SE, Hakim AM (2002) Toward wisdom from failure: lessons from neuroprotective stroke trials and new therapeutic directions. Stroke 33:2123–2136. CrossRef Medline

Hardingham GE, Fukunaga Y, Bading H (2002) Extrasynaptic NMDARs oppose synaptic NMDARs by triggering CREB shut-off and cell death pathways. Nat Neurosci 5:405– 414. Medline

Howitt J, Lackovic J, Low LH, Naguib A, Macintyre A, Goh CP, Callaway JK, Hammond V, Thomas T, Dixon M, Putz U, Silke J, Bartlett P, Yang B, Kumar S, Trotman LC, Tan SS (2012) Ndfip1 regulates nuclear Pten import in vivo to promote neuronal survival following cerebral ischemia. J Cell Biol 196:29–36. CrossRef Medline

Ikonomidou C, Turski L (2002) Why did NMDA receptor antagonists fail clinical trials for stroke and traumatic brain injury? Lancet Neurol 1:383–386. CrossRef Medline

Jurado S, Benoist M, Lario A, Knafo S, Petrok CN, Esteban JEA (2010) PTEN is recruited to the postsynaptic terminal for NMDA receptor-dependent long-term depression. EMBO J 29:2827–2840. CrossRef Medline

Koh JY, Choi DW (1987) Quantitative determination of glutamate mediated cortical neuronal injury in cell culture by lactate dehydrogenase efflux assay. J Neurosci Methods 20:83–90. CrossRef Medline

Lai TW, Shyu W-C, Wang YT (2011) Stroke intervention pathways: NMDA receptors and beyond. Trends in Mol Med 17:266–275. CrossRef Medline

Lee JO, Yang H, Georgescu MM, Di Cristofano A, Maehama T, Shi Y, Dixon JE, Pandolfi P, Pavletich NP (1999) Crystal structure of the PTEN tumor suppressor: implications for its phosphoinositide phosphatase activity and membrane association. Cell 99:323–334. CrossRef Medline

Leker R, Aharonowiz M, Greig NH, Ovadia H (2004) The role of p53-induced apoptosis in cerebral ischemia: effects of the p53 inhibitor pifithrin alpha. Exp Neurol 187:478–486. CrossRef Medline

Li J, Yen C, Liaw D, Podsypanina K, Bose S, Wang SI, Puc J, Miliaresis C, Rodgers L, McCombie R, Bigner SH, Giovanella BC, Ittmann M, Tycko B, Hibshoosh H, Wigler MH, Parsons R (1997) PTEN, a putative protein tyrosine phosphatase gene mutated in human brain, breast, and prostate cancer. Science 275:1943–1947. CrossRef Medline

Lipton P (1999) Ischemic cell death in brain neurons. Physiol Rev 79:1431–1568. Medline

Lipton SA, Rosenberg PA (1994) Excitatory amino acids as a final common pathway for neurologic disorders. N Engl J Med 330:613– 622. CrossRef Medline

Liu F, Wagner S, Campbell RB, Nickerson JA, Schiffer CA, Ross AH (2005) PTEN enters the nucleus by diffusion. J Cell Biochem 96:221–234. CrossRef Medline

Liu Y, Wong TP, Aarts M, Rooyakkers A, Liu L, Lai TW, Wu DC, Lu J, Tymianski M, Craig AM, Wang YT (2007) NMDA receptor subunits have differential roles in mediating excitotoxic neuronal death both in vitro and in vivo. J Neurosci 27:2846–2857. CrossRef Medline

Lo EH (2008) A new penumbra: transitioning from injury into repair after stroke. Nat Med 14:497–500. CrossRef Medline

Lucas DR, Newhouse JP (1957) The toxic effect of sodium L-glutamate on the inner layers of the retina. AMA Arch Ophthalmol 58:193–201. CrossRef Medline

Maehama T, Dixon JE (1998) The tumor suppressor, PTEN/MMAC1, dephosphorylates the lipid second messenger, phosphatidylinositol 3,4,5-trisphosphate. J Biol Chem 273:13375–13378. CrossRef Medline

Myers MP, Pass I, Batty IH, Van der Kaay J, Stolarov JP, Hemmings BA, Wigler MH, Downes CP, Tonks NK (1998) The lipid phosphatase activity of PTEN is critical for its tumor suppressor function. Proc Natl Acad Sci U S A 95:13513–13518. CrossRef Medline

Ning K, Pei L, Liao M, Liu B, Zhang Y, Jiang W, Mielke JG, Li L, Chen Y, El-Hayek YH, Fehlings MG, Zhang X, Liu F, Eubanks J, Wan Q (2004) Dual neuroprotective signaling mediated by downregulating two distinct phosphatase activities of PTEN. J Neurosci 24:4052–4060. CrossRef Medline

Okamoto SI, Pouladi MA, Talantova M, Yao D, Xia P, Ehrnhoefer DE, Zaidi R, Clemente A, Kaul M, Graham RK, Zhang D, Vincent Chen HS, Tong G, Hayden MR, Lipton SA (2009) Balance between synaptic versus extrasynaptic NMDA receptor activity influences inclusions and neurotoxicity of mutant huntingtin. Nat Med 15:1407–1413. CrossRef Medline

Olney JW (1969) Brain lesions, obesity, and other disturbances in mice treated with monosodium glutamate. Science 164:719–721. CrossRef Medline

Roesler R, Quevedo J, Schröder N (2003) Is it time to conclude that NMDA antagonists have failed? Lancet Neurol 2:13; discussion13. CrossRef Medline

Rothman SM (1983) Synaptic activity mediates death of hypoxic neurons. Science 220:536–537. CrossRef Medline

Rothman S (1984) Synaptic release of excitatory amino acid neurotransmitter mediates anoxic neuronal death. J Neurosci 4:1884–1891. Medline

Schwarze SR, Ho A, Vocero-Akbani A, Dowdy SF (1999) In vivo protein transduction: delivery of a biologically active protein into the mouse. Science 285:1569–1572. CrossRef Medline

Shen WH, Balajee AS, Wang J, Wu H, Eng C, Pandolfi PP, Yin Y (2007) Essential role for nuclear PTEN in maintaining chromosomal integrity. Cell 128:157–170. CrossRef Medline

Shyu WC, Lin SZ, Chiang MF, Chen DC, Su CY, Wang HJ, Liu RS, Tsai CH, Li H (2008) Secretoneurin promotes neuroprotection and neuronal plasticity via the Jak2/Stat3 pathway in murine models of stroke. J Clin Invest 118:133–148. CrossRef Medline

Simon RP, Swan JH, Griffiths T, Meldrum BS (1984) Blockade of *N*-methyl-D-aspartate receptors may protect against ischemic damage in the brain. Science 226:850–852. CrossRef Medline

Stambolic V, Suzuki A, de la Pompa de JL, Brothers GM, Mirtsos C, Sasaki T, Ruland J, Penninger JM, Siderovski DP, Mak TW (1998) Negative regulation of PKB/Akt-dependent cell survival by the tumor suppressor PTEN. Cell 95:29–39. CrossRef Medline

Steck PA, Pershouse MA, Jasser SA, Yung WK, Lin H, Ligon AH, Langford LA, Baumgard ML, Hattier T, Davis T, Frye C, Hu R, Swedlund B, Teng DH, Tavtigian SV (1997) Identification of a candidate tumour suppressor gene, MMAC1, at chromosome 10q23.3 that is mutated in multiple advanced cancers. Nat Genet 15:356–362. CrossRef Medline

Sun F, Park KK, Belin S, Wang D, Lu T, Chen G, Zhang K, Yeung C, Feng G, Yankner BA, He Z (2011) Sustained axon regeneration induced by co-deletion of PTEN and SOCS3. Nature 480:372–375. CrossRef Medline

Taghibiglou C, Martin HGS, Lai TW, Cho T, Prasad S, Kojic L, Lu J, Liu Y, Lo E, Zhang S, Wu JZZ, Li YP, Wen YH, Imm JH, Cynader MS, Wang YT (2009) Role of NMDA receptor-dependent activation of SREBP1 in excitotoxic and ischemic neuronal injuries. Nat Med 15:1399–1406. CrossRef Medline

Tang Y, Eng C (2006) PTEN autoregulates its expression by stabilization of p53 in a phosphatase-independent manner. Cancer Res 66:736–742. CrossRef Medline

Trotman LC, Wang X, Alimonti A, Chen Z, Teruya-Feldstein J, Yang H, Pavletich NP, Carver BS, Cordon-Cardo C, Erdjument-Bromage H, Tempst P, Chi SG, Kim HJ, Misteli T, Jiang X, Pandolfi PP (2007) Ubiquitination regulates PTEN nuclear import and tumor suppression. Cell 128:141–156. CrossRef Medline

Tu W, Xu X, Peng L, Zhong X, Zhang W, Soundarapandian MM, Balel C, Wang M, Jia N, Zhang W, Lew F, Chan SL, Chen Y, Lu Y (2010) DAPK1 interaction with NMDA receptor NR2B subunits mediates brain damage in stroke. Cell 140:222–234. CrossRef Medline

Vasko V, Saji M, Hardy E, Kruhlak M, Larin A, Savchenko V, Miyakawa M, Isozaki O, Murakami H, Tsushima T, Burman KD, De Micco C, Ringel MD (2004) Akt activation and localisation correlate with tumour invasion and oncogene expression in thyroid cancer. J Med Genet 41:161–170. CrossRef Medline

Walker SM, Leslie NR, Perera NM, Batty IH, Downes CP (2004) The tumour-suppressor function of PTEN requires an *N*-terminal lipid-binding motif. Biochem J 379:301–307. CrossRef Medline

Wang X, Trotman LC, Koppie T, Alimonti A, Chen Z, Gao Z, Wang J, Erdjument-Bromage H, Tempst P, Cordon-Cardo C, Pandolfi PP, Jiang X (2007) NEDD4–1 is a proto-oncogenic ubiquitin ligase for PTEN. Cell 128:129–139. CrossRef Medline

Wang Y, Ju W, Liu L, Fam S, D'Souza S, Taghibiglou C, Salter M, Wang YT (2004) alpha-amino-3-hydroxy-5-methylisoxazole-4-propionic acid subtype glutamate receptor (AMPAR) endocytosis is essential for *N*-methyl-D-aspartate-induced neuronal apoptosis. J Biol Chem 279: 41267–41270. CrossRef Medline

Whiteman DC, Zhou XP, Cummings MC, Pavey S, Hayward NK, Eng C (2002) Nuclear PTEN expression and clinicopathologic features in a population-based series of primary cutaneous melanoma. Int J Cancer 99:63–67. CrossRef Medline

Zheng M, Liao M, Cui T, Tian H, Fan DS, Wan Q (2012) Regulation of nuclear TDP-43 by NR2A-containing NMDA receptors and PTEN. J Cell Science 125:1556–1567. CrossRef Medline